Ion trap quantum gates with amplitude-modulated laser beams

Christian F Roos[1,2]

[1] Institut für Experimentalphysik, Universität Innsbruck, Technikerstr. 25, A-6020 Innsbruck, Austria
[2] Institut für Quantenoptik und Quanteninformation der Österreichischen Akademie der Wissenschaften, Otto-Hittmair-Platz 1, A-6020 Innsbruck, Austria
E-mail: Christian.Roos@uibk.ac.at

Abstract. In ion traps, entangling gate operations can be realized by a bichromatic pair of laser beams that collectively interact with the ions. In this paper, a new method of modelling the laser–ion interaction is introduced that turns out to be superior to standard techniques for the description of gate operations on optical qubits. The treatment allows for a comparison of the performance of gates based on $\sigma_z \otimes \sigma_z$ and $\sigma_\phi \otimes \sigma_\phi$ interactions on optical transitions where the bichromatic laser field can be realized by an amplitude-modulated laser resonant with the qubit transition. Shaping the amplitude of the bichromatic laser pulse is shown to make the gates more robust against experimental imperfections.

IOP Institute of Physics **ΦDPG** DEUTSCHE PHYSIKALISCHE GESELLSCHAFT

Contents

1. Introduction

The processing of information based on the laws of quantum physics [1] has become a very active field of research during the last decade. For the experimental demonstration of fundamental key results of quantum information theory, ion-trap based systems have played a major role. The success of ion trap experiments can be attributed to the fact that encoding quantum information in either hyperfine ground or meta-stable excited atomic states provides well-defined quantum bits (qubits) with long coherence times. The use of lasers for manipulating the qubit state allows for precisely switchable interactions with low decoherence rates. The fundamental operations of qubit initialization, arbitrary single qubit manipulation and quantum state-detection have already been used in atomic clocks with single ions for many years. Contrary to other realizations [1] of quantum information processing, the most demanding operation in ion traps consists of the realization of an entangling gate operation. Because of the repulsive Coulomb force, the inter-ion distance is orders of magnitude bigger than the characteristic length scale of any state-dependent interaction between ions in ground or low-lying excited states. In all current experiments creating entangled ions [2]–[5], gate operations rely on interactions that are mediated by the vibrational degrees of freedom of the ion string. These gate operations fall into two categories:

1. Quantum gates induced by a laser beam that interacts with a single ion at a time as originally proposed in the seminal paper by Cirac and Zoller [6] and later realized by the Innsbruck ion trapping group [2]. In these gates, a single ion is entangled with a vibrational mode [7] of the ion string and the entanglement is subsequently transferred from the vibrational mode to the internal state of a second ion.

2. Quantum gates induced by a bichromatic laser that collectively interacts with two or more ions. Here, a vibrational mode becomes transiently entangled with the qubits before getting disentangled at the end of the gate operation, resulting in an effective interactions between the qubits capable of entangling them. Gates of this type were first proposed by Milburn *et al* [8, 9], Sørensen and Mølmer [10, 11] and Solano *et al* [12], and subsequently realized by ion trapping groups in Boulder, Ann Arbor and Oxford [3]–[5].

Even though both classes of gates are applicable to hyperfine qubits as well as optical qubits (i.e. qubits encoded in hyperfine states or in states linked by a dipole-forbidden transition with an optical wavelength), current experiments with optical qubits have relied on the former and experiments with hyperfine qubits on the latter type of interaction. In any case, the main goal consists of demonstrating fast operations creating entanglement with high fidelity.

The purpose of the present paper is to discuss bichromatic gate operations with a focus on implementations using an optical transition. It turns out that for optical transitions, gate operations are achievable by illuminating the ions with an amplitude-modulated laser beam that is resonant with the qubit transition. The paper is organized as follows: section 2 reviews different methods of realizing bichromatic quantum gates and discusses properties that are specific to their application to optical qubits. In section 3, an effective Hamiltonian for the laser–ion interaction will be derived by going into a reference frame rotating at non-uniform speed in order to eliminate non-resonant excitations of the qubit transition that do not couple to the vibrational mode. In this way, it will be shown that for a single ion qubit the interaction is well described by a Hamiltonian $H = i\hbar(\gamma(t)a^\dagger - \gamma(t)^*a)\sigma_\psi$, where the coupling strength γ is proportional to the laser intensity in the limit of low intensities but starts to saturate at higher intensities and where $\sigma_\psi = \vec{\sigma} \cdot \vec{n}_\psi$ is a component of the Pauli spin operator $\vec{\sigma}$ coupling to a vibrational mode of the ion described by creation and annihilation operators $a^\dagger$, a. Furthermore, it will be shown that $\vec{n}_\psi$ depends not only on the particular type of gate operation but also on the laser intensity and the relative phase between the two frequencies of the bichromatic field. Equations (10), (17) and (27) describing the action of the gates based on $\sigma_z \otimes \sigma_z$ and on $\sigma_\phi \otimes \sigma_\phi$ (Mølmer–Sørensen) interactions are the key results of the paper. For the Mølmer–Sørensen gate, the result will be compared to the analysis presented in [11]. In addition, the performance of $\sigma_z \otimes \sigma_z$ and $\sigma_\phi \otimes \sigma_\phi$ gates will be compared. Section 4 shows how to use pulse-shaping of the laser intensity as well as spin echo techniques to make the gates more robust against fluctuations of the control parameters.

2. Quantum gate operations based on bichromatic laser fields

2.1. Driven quantum harmonic oscillator

The Hamiltonian $\tilde{H} = \hbar\nu a^\dagger a + \hbar\Omega i(a^\dagger e^{i\omega t} - a e^{-i\omega t})$ describes a harmonic oscillator oscillating at frequency ν and driven by a force with frequency ω and coupling strength Ω. Going into an interaction picture defined by $H_0 = \hbar\nu a^\dagger a$ yields the Hamiltonian $H = \hbar\Omega i(a^\dagger e^{i\delta t} - a e^{-i\delta t})$, where $\delta = \omega - \nu$. Under the action of the driving force, an oscillator that is initially in a coherent state remains in a coherent state. For a force that is slightly detuned from resonance, the coherent state maps out a circle in phase space and returns to the initial state after a period $\tau = 2\pi/\delta$. This operation multiplies the oscillator state by a phase factor whose magnitude is given by the ratio of the strength of the force and the detuning as shown in [3].

In order to allow for variations of the driving field's strength, we generalize the Hamiltonian to $H = i\hbar(\gamma(t)a^\dagger - \gamma^*(t)a)$ and calculate its propagator $U(t)$ by using the Baker–Campbell–Hausdorff relation $\hat{D}(\alpha)\hat{D}(\beta) = \hat{D}(\alpha + \beta)\exp(i\,\mathrm{Im}(\alpha\beta^*))$ for the displacement operator $\hat{D}(\alpha) = \mathrm{e}^{\alpha a^\dagger - \alpha^* a}$. For the propagator, we find

$$U(t) = \lim_{n\to\infty} \prod_{k=1}^{n} \exp\left(-\frac{i}{\hbar}H(t_k)\Delta t\right) = \hat{D}(\alpha(t))\exp(i\Phi(t)), \tag{1}$$

where $\Delta t = t/n$, $t_k = k\Delta t$ and

$$\alpha(t) = \int_0^t \mathrm{d}t'\,\gamma(t'), \quad \Phi(t) = \mathrm{Im}\int_0^t \mathrm{d}t'\,\gamma(t')\int_0^{t'} \mathrm{d}t''\,\gamma^*(t'').$$

In the case of a driving force with constant amplitude, $\gamma(t) = \Omega\mathrm{e}^{i\delta t}$, one obtains $\alpha(t) = i\left(\frac{\Omega}{\delta}\right)(1 - \mathrm{e}^{i\delta t})$ and $\Phi = \left(\frac{\Omega}{\delta}\right)^2(\delta t - \sin\delta t)$. After a time $\tau_N = 2\pi N/|\delta|$, $N = 1, 2, \ldots$, the coherent state returns to its initial state in phase space with its phase changed by an amount $\Phi(\tau_N) = 2\pi N\left(\frac{\Omega}{\delta}\right)^2\mathrm{sign}(\delta)$. By making this phase change depend on the internal states of a pair of ions, an entangling gate operation can be achieved. For

$$H = i\hbar(\gamma(t)a^\dagger - \gamma^*(t)a)\mathcal{O}, \tag{2}$$

where $\mathcal{O}$ is an operator acting on the qubit states, the propagator (1) is replaced by

$$U_\gamma(t) = \hat{D}(\alpha(t)\mathcal{O})\exp(i\Phi(t)\mathcal{O}^2). \tag{3}$$

Choosing the interaction time τ such that $\alpha(\tau) = 0$ thus realizes a propagator that depends nonlinearly on $\mathcal{O}$ and does not alter the vibrational state.

2.2. Laser–ion interaction

The interaction of a single ion qubit resonantly excited by a monochromatic laser field with frequency ω_L is usually described by performing a rotating-wave approximation with respect to the optical frequency to obtain the Hamiltonian

$$H = \hbar\Omega\sigma_+\mathrm{e}^{-i\delta t}\mathrm{e}^{i\eta(a\mathrm{e}^{-i\nu t} + a^\dagger\mathrm{e}^{i\nu t})} + \mathrm{h.c.}, \tag{4}$$

here, $\delta = \omega_\mathrm{L} - \omega_0$ is the detuning from the qubit transition frequency ω_0, ν is the frequency of the ion's vibrational mode of interest, and $\sigma_+ = (\sigma_x + i\sigma_y)/2$ with the Pauli matrices $\sigma_{x,y}$. The strength of the laser–ion coupling is characterized by the Rabi frequency Ω, and the strength of processes involving changes in the vibrational state is determined by the value of the Lamb–Dicke parameter η. Equation (4) represents a Hamiltonian in an interaction picture that is defined with respect to the Hamiltonian $H_0 = \hbar\nu a^\dagger a + (\hbar\omega_0/2)\sigma_z$ describing the ion qubit in the absence of any laser–ion interactions. If $\eta \ll 1$, the Lamb–Dicke approximation $\mathrm{e}^{i\eta(a\mathrm{e}^{-i\nu t} + a^\dagger\mathrm{e}^{i\nu t})} \approx 1 + i\eta(a\mathrm{e}^{-i\nu t} + a^\dagger\mathrm{e}^{i\nu t})$ is used to simplify equation (4). The resulting three terms describe excitations on the carrier, the lower and the upper motional sideband, respectively. The generalization of the Hamiltonian to the case of two and more ions is straightforward. For the sake of simplicity, calculations in section 3 will be limited to the case of the laser coupling to the centre-of-mass mode along the axis of the ion string where all ions experience the same coupling strength. A detailed account of laser–ion interactions is given in [13].
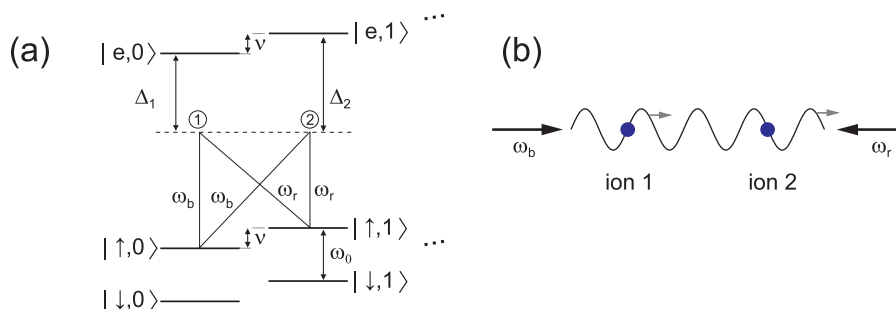
Figure 1. Raman coupling of motional states for a hyperfine or Zeeman qubit. (a) The states $|\uparrow, n = 0\rangle$ and $|\uparrow, n = 1\rangle$ are coupled via the excited state $|e\rangle$. A similar coupling not shown in the figure exists for the qubit state $|\downarrow\rangle$. The laser detunings Δ_1 and Δ_2 from the mediating states are large compared with trap frequency ν and the qubit level spacing ω_0 to avoid spontaneous emission from state $|e\rangle$. Constructive interference of paths 1 and 2 is achieved for counter-propagating laser beams. (b) The coupling is maximized for counter-propagating laser beams with frequencies ω_b and ω_r forming a moving standing wave along the axis of vibration of the motional mode of interest.

2.3. $\sigma_z \otimes \sigma_z$ gate

A Hamiltonian as described by equation (2) was employed for the first time in an experiment [14] creating a Schrödinger cat state with a single ion using $\mathcal{O} = \sigma_z$, i.e. a coupling to the motional mode that depended on the internal energy eigenstate of the ion. Later, it was realized that the same type of coupling could be used to entangle a pair of ions by performing a conditional phase gate [3, 9]. In the experimental realizations [3, 5], spin-dependent forces acting on a pair of hyperfine or Zeeman ground states have been realized by near resonant driving of Raman transitions between vibrational states (see figure 1). For this purpose, two non-copropagating laser beams with frequencies ω_b, ω_r form a moving standing wave with difference frequency $\omega_b - \omega_r$ close to the frequency ν of a vibrational mode. The ac-Stark shift of the qubit states $|\downarrow\rangle$, $|\uparrow\rangle$ results from a non-resonant coupling to another atomic state $|e\rangle$ that is made qubit state-dependent by properly chosen polarizations. Since the laser field exhibits a strong spatiotemporal modulation, the resulting potential gradients induce a force acting on the qubits that is state-dependent and that couples to the vibrational mode by displacing the qubit along a circle in phase space. When the ions couple to the centre-of-mass mode (stretch mode), the coupling to the mode can be made to disappear when both qubits are in the same quantum state by choosing an ion spacing that is an odd (even) integer multiple of half the wavelength of the moving standing wave. Disregarding unimportant global and single qubit phases, this coupling is then described by an operator $\mathcal{O} = S_z$ where $S_z = \sigma_z^{(1)} + \sigma_z^{(2)}$ is a collective spin component of the qubits.

The situation is different for qubits encoded in atomic states connected by a narrow optical transition. For coupling motional states $|\downarrow, n = 0\rangle \leftrightarrow |\downarrow, n = 1\rangle$, here, the other qubit state $|\uparrow\rangle$ serves to mediate the coupling. Similarly, a coupling between the states $|\uparrow, n = 0\rangle \leftrightarrow |\uparrow, n = 1\rangle$ is mediated by the state $|\downarrow\rangle$. To achieve a strong coupling, a detuning Δ_i from the intermediate states can be chosen that is smaller than the transition frequency between vibrational states provided that the decay rate of the metastable state is small compared
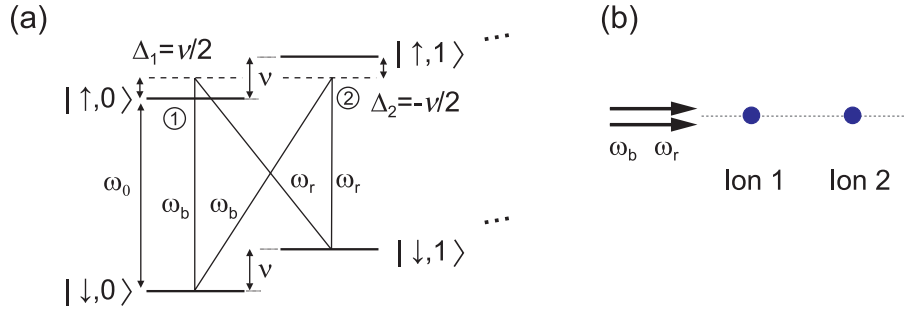
Figure 2. Raman coupling of motional states for an optical qubit. (a) The coupling for states $|\uparrow, n = 0\rangle$ and $|\uparrow, n = 1\rangle$ is mediated by the states $|\downarrow, n = 0\rangle$ and $|\downarrow, n = 1\rangle$ and vice versa on the narrow qubit transition. Since spontaneous scattering from the mediating state is small, the detuning can be made small compared to the trap frequency. For $\Delta_1 = \nu/2$ and $\Delta_2 = -\nu/2$, the coupling is maximized by choosing a copropagating beam geometry. (b) Optimum coupling is achieved for co-propagating laser beams with frequencies ω_b and ω_r propagating along the axis of vibration of the motional mode of interest. As the bichromatic laser field could also be described by a monochromatic laser field that is amplitude-modulated with a frequency $\omega_b - \omega_r$ close to the vibrational frequency, no spatially varying ac-Stark shifts are involved in the coupling.

to ν. For $\omega_{b,r} = \omega_0 \pm \nu/2$, the two interfering paths shown in figure 2(a) connecting levels $|\downarrow, n = 0\rangle \leftrightarrow |\downarrow, n = 1\rangle$ have equal strength. Since the detunings from the mediating states now have opposite signs, destructive interference is achieved for counter-propagating beams whereas the coupling is maximized for co-propagating beams [17]. In the limit of small excitation ($\Omega \ll \nu$), the coupling strength $\Omega_{R,0}$ on the Raman transition between $|\downarrow, n = 0\rangle$ and $|\downarrow, n = 1\rangle$ is given by $\Omega_{R,0} = 2\eta\Omega^2/\nu$. The states $|\uparrow, n = 0\rangle$ and $|\uparrow, n = 1\rangle$ are coupled with equal strength but opposite sign. For stronger excitation, the carrier transition is non-resonantly excited which leads to a saturation of $\Omega_{R,0}$. As long as the intensities of the bichromatic beams are equal, there is no overall ac-Stark shift due to excitation of the carrier transition and the first motional sidebands because ac-Stark shifts caused by the two laser fields exactly cancel each other.

In the case of two ions excited on the centre-of-mass mode, a driven quantum mechanical oscillator is realized with collective atomic oscillator $\mathcal{O} = S_z$. In addition to the coupling of vibrational states, there is another small Mølmer–Sørensen coupling [10] that does not exist for the case of hyperfine or Zeeman qubits: collective spin flips between the states $|\downarrow\downarrow, n\rangle$ and $|\uparrow\uparrow, n\rangle$ occur by processes involving a blue and a red photon that are mediated by the states $|\downarrow\uparrow, n \pm 1\rangle$ and $|\uparrow\downarrow, n \pm 1\rangle$ (see figure 3). A similar process involving either two blue or two red photons couples the states $|\uparrow\downarrow, n\rangle$ and $|\downarrow\uparrow, n\rangle$.

2.4. $\sigma_\phi \otimes \sigma_\phi$ gate

In contrast to $\sigma_z \otimes \sigma_z$ gates that do not change the internal states of the ions, the $\sigma_\phi \otimes \sigma_\phi$ gate operations first investigated by Sørensen and Mølmer [10] and others [12] relies on collective
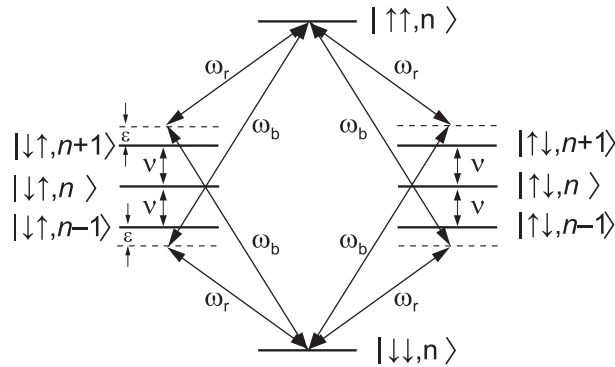
Figure 3. Mølmer–Sørensen gate. A bichromatic laser field with frequencies ω_b, ω_r satisfying $2\omega_0 = \omega_b + \omega_r$ is tuned close to the upper and lower motional sideband of the qubit transition. The field couples the qubit states $|\downarrow\downarrow\rangle \leftrightarrow |\uparrow\uparrow\rangle$ via the four interfering paths shown in the figure. Similar processes couple the states $|\uparrow\downarrow\rangle \leftrightarrow |\downarrow\uparrow\rangle$ with the same strength provided that the Rabi frequencies of the light fields ω_b and ω_r are equal.

spin flips $|\downarrow\downarrow\rangle \leftrightarrow |\uparrow\uparrow\rangle$, $|\downarrow\uparrow\rangle \leftrightarrow |\downarrow\uparrow\rangle$ by processes coupling to the lower and upper motional sidebands as illustrated in figure 3. It can be seen that the Hamiltonian governing the action of the gate is described by setting $\mathcal{O} = \cos\phi\, S_x + \sin\phi\, S_y$ [15, 16]. For a properly chosen coupling strength, the gate operations maps the product state basis $\{|\uparrow\uparrow\rangle, |\uparrow\downarrow\rangle, |\downarrow\uparrow\rangle, |\downarrow\downarrow\rangle\}$ on to a basis of entangled states. For hyperfine qubits, a detailed discussion of advantageous beam geometries is presented in [18]. In the case of optical qubits, it is again possible to choose a pair of co-propagating beams for performing the gate operation. The only difference to the $\sigma_z \otimes \sigma_z$ gate consists of the choice of laser frequencies $\omega_{b,r} = \omega_0 \pm \nu$ required for achieving a resonant coupling. Formally, the gate operation is equivalent to a $\sigma_z \otimes \sigma_z$ interaction in a rotated basis. To stress this analogy, the Mølmer–Sørensen gate operation is often also called a $\sigma_\phi \otimes \sigma_\phi$ gate.

The possibility of choosing co-propagating laser beams for performing either $\sigma_z \otimes \sigma_z$ or $\sigma_\phi \otimes \sigma_\phi$ gates is attractive from an experimental point of view. The light field could be generated by passing a laser beam through an acousto–optical modulator driven by two radio-frequency fields and subsequently coupling the first-order diffracted beams into a single-mode optical fibre, thus realizing a simple and stable set-up[3]. If the Rabi frequencies Ω_b and Ω_r of the blue and the red detuned laser beam are equal, light shifts due to the non-resonant excitation of the carrier transition and the first-order sidebands are exactly cancelled. Light shifts arising from coupling to other Zeeman transitions or far-detuned dipole transitions could be cancelled by suitably balancing the ratio Ω_b / Ω_r.

---

[3] In principle, $\sigma_\phi \otimes \sigma_\phi$ gate operations could also be achieved by phase-modulating a laser with a modulation frequency close to ν by choosing a modulation index where the carrier strength vanishes. However, this approach has the strong disadvantage that even small changes of the modulation index from the desired value give rise to light resonant with the transition which is having disastrous effects on the gate performance. Similarly, modulating at frequency close to 2ν and using the carrier and one of the first sidebands is problematic because of light shifts induced by the other sidebands.

3. Effective Hamiltonians for $\sigma_z \otimes \sigma_z$ and $\sigma_\phi \otimes \sigma_\phi$ gates

We are interested in deriving an effective Hamiltonian that accurately describes the dynamics on a pair of optical qubits induced by a co-propagating bichromatic laser field with frequencies $\omega_{b,r} = \omega_0 \pm \delta$, where the detuning is either close to half the vibrational frequency or close to the vibrational frequency, i.e. $\delta = (\nu - \epsilon)/2$ or $\delta = \nu - \epsilon$ with $\epsilon \ll \nu$. As optical qubits interacting with lasers typically have smaller Lamb–Dicke parameters than hyperfine qubits coupled by Raman transitions, transient non-resonant excitation of the carrier transition is expected to play an important role for $\Omega \lesssim \nu$. Whereas usually non-resonant interactions are taken into account only qualitatively after having derived an effective Hamiltonian, in the following calculation they will be eliminated right at the beginning by going into a reference frame rotating at non-uniform speed.

The Hamiltonian for the bichromatic laser field we are interested in, is given by

$$H = \hbar\Omega e^{-i\phi} S_+ (e^{-i(\delta t + \zeta)} + e^{i(\delta t + \zeta)}) e^{i\eta(ae^{-i\nu t} + a^\dagger e^{i\nu t})} + \text{h.c.} \tag{5}$$

The laser is assumed to interact collectively with m ions on the axial centre-of-mass mode. Here, $S_+ = \sum_{i=1}^m \sigma_+^{(i)}$, and $a, a^\dagger$ denote operators annihilating and creating phonons. It is also possible to interpret this interaction as being due to a single resonant laser beam that is amplitude-modulated with modulation frequency δ. The optical phase of the laser field is denoted ϕ, and the phase ζ accounts for a time difference between the start of the gate operation and the maximum of the amplitude modulation on the laser beam. Using the picture of an amplitude-modulated resonant beam, it is obvious that there are fast dynamical processes on the carrier transition with a periodicity given by $\tau = 2\pi/\delta$ that excite the ions to the other state in the first half of the period and transfer it back to the original state in the second half. We are not really interested in exactly calculating the dynamical evolution of the quantum state on this fast timescale. Rather, we would like to know the time evolution at the instances $\tau, 2\tau, 3\tau, \ldots, \tau = 2\pi/\delta$. It is useful to rewrite (5) as

$$H = \hbar f(t)(e^{-i\phi} S_+ \hat{D}(i\eta e^{i\nu t}) + e^{i\phi} S_- \hat{D}(-i\eta e^{i\nu t}))$$

$$= \hbar f(t)((S_x \cos\phi + S_y \sin\phi)(D_+ + D_-) + i(S_y \cos\phi - S_x \sin\phi)(D_+ - D_-))$$

$$=: \hbar f(t)(S_x^{(\phi)}(D_+ + D_-) + iS_y^{(\phi)}(D_+ - D_-)),$$

where we used the displacement operator $\hat{D}(\alpha) = e^{\alpha a^\dagger - a^* a}$ and the definitions $D_\pm = \hat{D}(\pm i\eta e^{i\nu t})/2$, $S_x^{(\phi)} = S_x \cos\phi + S_y \sin\phi$, $S_y^{(\phi)} = S_y \cos\phi - S_x \sin\phi$ and $f(t) = 2\Omega\cos(\delta t + \zeta)$. For $\delta = \nu/2$ or $\delta = \nu$ as required by either $\sigma_z \otimes \sigma_z$ or $\sigma_\phi \otimes \sigma_\phi$ interactions, the Hamiltonian is periodic in time, i.e. $H(t + \tau) = H(t)$ with period $\tau = 2\pi/\delta$. Note that we assume the two-photon couplings to be strictly resonant for the moment. In the next step, we will get rid of the fast non-resonant carrier oscillation by going into another interaction picture defined by $H_0 = \hbar f(t) S_x^{(\phi)}$. Writing

$$H = \hbar f(t) S_x^{(\phi)} + H_1,$$

with

$$H_1 = \hbar f(t)(S_x^{(\phi)}(D_+ + D_- - 1) + iS_y^{(\phi)}(D_+ - D_-)),$$

we obtain the interaction Hamiltonian

$$H_I = e^{iF(t)S_x^{(\phi)}} H_1 e^{-iF(t)S_x^{(\phi)}}$$

$$= \hbar f(t) S_x^{(\phi)}(D_+ + D_- - 1) + \hbar f(t)\left(\cos(2F(t))S_y^{(\phi)} - \sin(2F(t))S_z\right) i(D_+ - D_-),$$

where

$$F(t) = \frac{2\Omega}{\delta}(\sin(\delta t + \zeta) - \sin \zeta). \tag{6}$$

Now, we can approximate the time evolution over the course of an oscillation period by a Magnus expansion of the propagator [19] in order to obtain

$$U_I(t) = \exp\left\{ -\frac{i}{\hbar}\left(\int_0^t dt' H_I(t') - \frac{i}{2\hbar} \int_0^t dt' \int_0^{t'} dt'' [H_I(t'), H_I(t'')] + \cdots \right) \right\}. \tag{7}$$

From now on, the phase ϕ will be set to zero to simplify the notation. The formulae in the remainder of section 3 are easily generalized to the case of arbitrary ϕ by making the replacements $S_x \to S_x^{(\phi)}$ and $S_y \to S_y^{(\phi)}$.

In the following two subsections, effective Hamiltonians for the $\sigma_z \otimes \sigma_z$ gate and the $\sigma_\phi \otimes \sigma_\phi$ gate will be derived starting from equation (7). We are interested in obtaining Hamiltonians of the form given in equation (2) that are valid in the regime $\Omega \ll \nu$. In addition, the calculation is going to yield correction terms for the case when $\Omega \ll \nu$ no longer strictly holds and additional terms that do not commute with the atomic operator $\mathcal{O}$ in equation (2). Towards this aim, terms proportional to higher orders of the expansion parameter (Ω/δ) will be dropped. In the calculation, Bessel functions $J_n(x)$ will be evaluated at $x = 4\Omega/\delta$. These functions will be kept till the end of the calculation and expanded in Ω/δ only for the final analysis.

3.1. $\sigma_z \otimes \sigma_z$ gate

For the $\sigma_z \otimes \sigma_z$ gate, we set $\delta = \nu/2$. We start by calculating the first term $H_{eff}^{(I,1)} = \frac{1}{\tau}\int_0^\tau dt' H_I(t')$ appearing in the exponent of (7). Here, it is important to note that the integrand $H_I(t) = \sum_{k=-\infty}^{\infty} H_{(k)}e^{ik\delta t}$ is a periodic function of time with period $\tau = 2\pi/\delta$ so that all its Fourier components except the constant term $H_{(0)}$ will average to zero when they are integrated over one period. The only non-zero Fourier components of the function $f(t) = \Omega(e^{i(\delta t + \zeta)} + e^{-i(\delta t + \zeta)}) = \sum_{n=-\infty}^{\infty} f_n e^{in\delta t}$ are $f_{+1} = \Omega e^{i\zeta}$ and $f_{-1} = \Omega e^{-i\zeta}$. Since all non-zero Fourier components of $(D_+ + D_- - 1)$ are even integer multiples of δ, the S_x-term of H_I averages to zero. Therefore, we obtain

$$H_{eff}^{(I,1)} = \frac{\hbar}{\tau}\int_0^\tau dt\, f(t)\left(\cos(2F(t))S_y - \sin(2F(t))S_z\right) i(D_+ - D_-).$$

In the Lamb–Dicke limit,

$$i(D_+ - D_-) \approx -\eta(a e^{-i2\delta t} + a^\dagger e^{i2\delta t}) =: \sum_{n=-\infty}^{\infty} d_n e^{in\delta t},$$

and the components $d_{+2} = -\eta a^\dagger$ and $d_{-2} = -\eta a$ are the only relevant ones. Finally, we have

$$\cos(2F(t))S_y - \sin(2F(t))S_z = \tfrac{1}{2}\left[e^{i2F(t)}(S_y + iS_z) + e^{-i2F(t)}(S_y - iS_z)\right]$$

$$= Ae^{i(4\Omega/\delta)\sin(\delta t + \zeta)} + A^\dagger e^{-i(4\Omega/\delta)\sin(\delta t + \zeta)}$$

$$= \sum_{n=-\infty}^{\infty}\left(AJ_n\left(\frac{4\Omega}{\delta}\right) + A^\dagger J_n\left(-\frac{4\Omega}{\delta}\right)\right)e^{in\zeta}e^{in\delta t} =: \sum_{n=-\infty}^{\infty} a_n e^{in\delta t},$$

where J_n is a Bessel function, $A = \tfrac{1}{2}(S_y + iS_z)e^{-i\psi}$ with

$$\psi = \frac{4\Omega}{\delta}\sin\zeta, \tag{8}$$

and $a_n = (AJ_n(\frac{4\Omega}{\delta}) + A^\dagger J_n(-\frac{4\Omega}{\delta}))e^{in\zeta} = (A + (-1)^n A^\dagger)J_n(\frac{4\Omega}{\delta})e^{in\zeta}$. In the following, the argument $4\Omega/\delta$ of the Bessel functions J_n will often be dropped to keep the notation simple. It is convenient to express $A \pm A^\dagger$ as

$$S_{y,\psi} := S_y\cos\psi + S_z\sin\psi = A + A^\dagger, \quad S_{z,\psi} := S_z\cos\psi - S_y\sin\psi = -i(A - A^\dagger). \tag{9}$$

Note that the linear transformation (9) preserves the usual Lie algebra commutation relations for the operators S_x, $S_{y,\psi}$ and $S_{z,\psi}$. The four terms $f_{+1}d_{-2}a_{+1}, f_{-1}d_{+2}a_{-1}$, and to a lesser degree $f_{+1}d_{+2}a_{-3}$, $f_{-1}d_{-2}a_{+3}$, contribute to $H_{\text{eff}}^{(\text{I})}$. Evaluating

$$f_{+1}d_{-2}a_{+1} = (\Omega e^{i\zeta})(-\eta a)(A - A^\dagger)J_1\left(\frac{4\Omega}{\delta}\right)e^{i\zeta} = -\eta\Omega J_1 e^{2i\zeta}iaS_{z,\psi},$$

as well as the other terms, we arrive at the effective Hamiltonian

$$H_{\text{eff}}^{(\text{I},1)} = i\hbar\eta\Omega(J_1 + J_3)(e^{-2i\zeta}a^\dagger - e^{2i\zeta}a)S_{z,\psi},$$

where $\eta\Omega(J_1 + J_3) \approx (2\eta\Omega^2/\delta)(1 - 4\Omega^2/(3\delta^2))$. This Hamiltonian describes a spin-dependent force that starts to saturate when the Rabi frequency goes up. While the atomic operator $\mathcal{O} = S_{z,\psi}$ coincides in the limit of weak excitation with the operator S_z obtained from second-order perturbation theory, it depends on the phase ζ between the blue- and the red-detuned laser beams in the limit of strong excitation. For the periodic Hamiltonian $H_{\text{I}}(t) = \sum_{k=-\infty}^{\infty} H_k e^{ik\delta t}$, the second-order contribution to the effective Hamiltonian $H_{\text{eff}}^{(\text{I})}$ is given by

$$H_{\text{eff}}^{(\text{I},2)} = \frac{1}{\hbar\delta}\sum_{m=1}^{\infty}\frac{1}{m}[H_{(m)}, H_{(-m)}].$$

After evaluating the commutators $[H_{(1)}, H_{(-1)}]$, $[H_{(3)}, H_{(-3)}]$, the effective Hamiltonian

$$H_{\text{eff}}^{(\text{I})} = i\hbar\eta\Omega(J_1 + J_3)S_{z,\psi}(a^\dagger e^{-2i\zeta} - ae^{2i\zeta}) - \frac{4\hbar\eta^2\Omega^2}{3\delta}J_0^2 S_{y,\psi}^2$$

is obtained (the contribution of the commutator $[H_{(2)}, H_{(-2)}] \propto (\eta\Omega)^2(\Omega/\delta)^6$ is insignificant). If the detuning $\delta = (\nu - \epsilon)/2$ slightly deviates from half the oscillation frequency ν, the Hamiltonian

$$H_{\text{eff}}^{(\text{I})} = i\hbar\eta\Omega(J_1 + J_3)S_{z,\psi}(a^\dagger e^{i(\epsilon t - 2\zeta)} - ae^{-i(\epsilon t - 2\zeta)}) - \frac{4\hbar\eta^2\Omega^2}{3\delta}J_0^2 S_{y,\psi}^2 \tag{10}$$

is obtained. The second-order term $H_{\mathrm{eff}}^{(\mathrm{I},2)}$ accounts for collective spin flip processes caused by a Mølmer–Sørensen interaction. If this interaction did not exist, the propagator could be calculated in the same way as for the driven harmonic oscillator described by (2). In the limit $\Omega \ll \nu$, where $\eta\Omega(J_1 + J_3) = 2\eta\Omega^2/\delta + O(\Omega^4)$, the time evolution from $\mathrm{t} = 0$ to $t^* = 2\pi/|\epsilon|$ would create a mapping of quantum states $\phi(0) \to \phi(t^*)$ described by the operator

$$U_{\mathrm{I}}(t^*) = \exp(\mathrm{i}\theta t^* S_{z,\psi}^2),$$

with

$$\theta t^* = \frac{\pi}{2}\left(\frac{4\eta\Omega^2}{\epsilon\delta}\right)^2 \mathrm{sign}(\epsilon).$$

For $m = 2$ ions, the operator $U_{\mathrm{I}}(t^*)$ performs a conditional phase gate if $\theta t^* = \pi/8$. For $\zeta = 0$ and weak excitation ($\Omega \ll \nu$), this requires setting the coupling strength $\Omega = \Omega_{\mathrm{c}}$ with

$$\Omega_{\mathrm{c}}^2 = \frac{|\epsilon|\delta}{8\eta}. \tag{11}$$

In the limit where $\Omega \ll \nu$ no longer holds, saturation effects reduce the geometric phase Φ picked up in the gate operation. For $\Omega = \Omega_{\mathrm{c}}$, we would now have

$$\theta t^* \approx \frac{\pi}{8}\left(1 - \frac{2}{3\eta N_{\mathrm{t}}}\right), \tag{12}$$

where $N_{\mathrm{t}} = \nu/|\epsilon|$ counts the number of trap cycles during the gate operation. For $\eta = 0.1$ and a gate time of 100 trap cycles, Φ is reduced by about 7%. The smaller the Lamb–Dicke factor gets, the more important saturation effects become for a given gate time. The Mølmer–Sørensen interaction contributes a term to the propagator $U_{\mathrm{I}}(t^*)$ which is now approximately described by

$$U_{\mathrm{I}}(t^*) \approx \exp(\mathrm{i}\theta t^* S_{z,\psi}^2)\exp(\mathrm{i}\kappa t^* S_{y,\psi}^2), \tag{13}$$

with

$$\kappa t^* = \frac{\pi}{2}\left(\frac{4\eta\Omega^2}{\epsilon\delta}\right)^2 \frac{|\epsilon|\delta}{3\Omega^2}. \tag{14}$$

For the ratio κ/θ,

$$\left|\frac{\kappa}{\theta}\right| = \frac{8}{3}\eta. \tag{15}$$

If $\eta \ll 1$, the contribution from the second term $\propto S_{y,\psi}^2$ is comparatively small.

Up to now, we have disregarded the fact that the effective Hamiltonian is valid only for times $T = \frac{2\pi}{\delta}N$, where $N = 1, 2, \ldots$ and $\delta = \frac{1}{2}(\nu - \epsilon)$. Therefore, the gate time T needs to fulfil $|\epsilon|T = 2\pi$ as well as $\delta T = 2\pi N$, with integer N. Combining both conditions, we find

$$\epsilon = \frac{\nu}{2N+1}, \qquad N \in \mathbb{N}.$$

In writing equation (13), terms arising from the non-vanishing commutator $[S_{z,\psi}, S_{y,\psi}^2]$ were neglected. Using the abbreviations $\Omega_{\mathrm{m}} = \eta\Omega(J_1 + J_3)$ and $\Omega_{\mathrm{MS}} = 4\eta^2\Omega^2 J_0^2/(3\delta)$, it is

convenient to rewrite $H_{\text{eff}}^{(\text{I})} = H_A + H_B$ with

$$H_A = \hbar\Omega_{\text{m}} \text{i} S_{z,\psi} (a^\dagger e^{\text{i}(\epsilon t - 2\zeta)} - a e^{-\text{i}(\epsilon t - 2\zeta)}) - \frac{\hbar\Omega_{\text{MS}}}{2}(S_x^2 + S_{y,\psi}^2),$$

$$H_B = \frac{\hbar\Omega_{\text{MS}}}{2}(S_x^2 - S_{y,\psi}^2),$$

since H_A and H_B commute. The time evolution induced by H_A is given by the propagator

$$U_A(t) = \hat{D}(\lambda(t)S_{z,\psi})\exp(\text{i}\Phi(t)S_{z,\psi}^2)\exp\left(\text{i}\frac{\Omega_{\text{MS}}t}{2}(S_x^2 + S_{y,\psi}^2)\right), \tag{16}$$

with $\lambda(t) = -\text{i}e^{-\text{i}2\zeta}(\Omega_{\text{m}}/\epsilon)(e^{\text{i}\epsilon t} - 1)$ and $\Phi(t) = (\Omega_{\text{m}}/\epsilon)^2(\epsilon t - \sin(\epsilon t))$, and for the interaction Hamiltonian $H_{\text{I},B} = U_A^\dagger H_B U_A$ one finds

$$H_{\text{I},B} = \frac{\hbar\Omega_{\text{MS}}}{2}(\hat{C}(4\lambda(t))(S_x^2 - S_{y,\psi}^2) + \hat{S}(4\lambda(t))\{S_x, S_{y,\psi}\}).$$

Here, the displacement operator $\hat{D}(\pm\alpha) = \hat{C}(\alpha) \pm \text{i}\hat{S}(\alpha)$ was expressed by the real-valued operators $\hat{C}$ and $\hat{S}$. For the special case $\zeta = 0$ this is equivalent to

$$H_{\text{I},B} = \frac{\hbar\Omega_{\text{MS}}}{4}(\hat{D}(-4\lambda(t))S_+^2 + \hat{D}(4\lambda(t))S_-^2).$$

The last expression shows that the interaction Hamiltonian $H_{\text{I},B}$ describes collective spin flips between the levels $|\downarrow\downarrow\rangle$ and $|\uparrow\uparrow\rangle$ that go along with displacements of the vibrational state. For a phase gate operation, $\max(|4\lambda(t)|) \approx 2$. Minimum uncertainty states of motion are not conserved by the interaction.

3.2. Mølmer–Sørensen gate operation

The formalism developed so far can be employed to study the Mølmer–Sørensen gate as Hamiltonian (5) also describes the bichromatic laser field of the Mølmer–Sørensen gate. Since the laser frequencies are set close to the blue and red sideband resonance, the only difference is that $\delta = \nu - \epsilon$ instead of $\delta = (1/2)(\nu - \epsilon)$, thus changing the values of the Fourier components d_n used to express $D_\pm$. Taking into account the leading terms in first and second order for the calculation of (7), one finds the effective Hamiltonian

$$\frac{H_{\text{eff}}^{(\text{I})}}{\hbar} = -\eta\Omega(J_0 + J_2)S_{y,\psi}(a^\dagger e^{\text{i}(\epsilon t - \zeta)} + a e^{-\text{i}(\epsilon t - \zeta)}) - \frac{\eta^2\Omega^2}{2\delta}J_0^2 S_{y,\psi}^2 + \frac{2\eta^2\Omega^2}{3\delta}J_1^2 S_{z,\psi}^2, \tag{17}$$

instead of (10). Integrating from $t = 0$ to $t^* = \frac{2\pi}{|\epsilon|}$ and neglecting commutators involving $S_{z,\psi}$ in the Magnus expansion, yields the propagator

$$U_{\text{I}}(t^*) \approx \exp\left\{\text{i}t^*\left(\left(\frac{\eta^2\Omega^2}{\epsilon}\left((J_0 + J_2)^2 + \frac{\eta^2\Omega^2}{2\delta}J_0^2\right)\right)S_{y,\psi}^2 - \frac{2\eta^2\Omega^2}{3\delta}J_1^2 S_{z,\psi}^2\right)\right\}$$

$$= \exp(\text{i}\lambda t^* S_{y,\psi}^2)\exp(-\text{i}\mu t^* S_{z,\psi}^2), \tag{18}$$

with

$$\lambda t^* = \pi\frac{2\eta^2\Omega^2}{\epsilon|\epsilon|}\left((J_0 + J_2)^2 + (\epsilon/2\delta)J_0^2\right), \tag{19}$$

$$\mu t^* \approx \pi \frac{16\eta^2\Omega^4}{3|\epsilon|\delta^3}. \tag{20}$$

The contribution $\propto 1/(2\delta)$ comes from the counter-rotating term, the red laser coupling to the blue sideband and vice versa. For weak excitation, we have

$$U_{\mathrm{I}}(t^*) = \exp\left\{\mathrm{i}\pi \frac{2\eta^2\Omega^2}{\epsilon|\epsilon|} S_{y,\psi}^2\right\}.$$

For $m = 2$ ions, an entangling gate operation is achieved by setting $|\lambda t^*| = \frac{\pi}{8}$ which amounts to setting the coupling strength Ω to

$$\Omega_{\mathrm{c}} = \frac{|\epsilon|}{4\eta}. \tag{21}$$

In the limit where $\Omega \ll \nu$ is no longer valid but where $|\epsilon/\eta| \ll \nu$ still holds, we find for the correction terms in (19) when keeping $\Omega = \Omega_{\mathrm{c}}$

$$|\lambda t^*| \approx \frac{\pi}{8}\left(1 - \frac{1}{4(\eta N_{\mathrm{t}})^2} - \frac{\mathrm{sign}(\epsilon)}{2N_{\mathrm{t}}}\right). \tag{22}$$

and for the ratio

$$\left|\frac{\mu}{\lambda}\right| \approx \frac{1}{6(\eta N_{\mathrm{t}})^2 N_{\mathrm{t}}}. \tag{23}$$

For $\eta = 0.1$ and a gate operation that is performed within 100 trap cycles, the correction terms to λt^* have a relative strength of 0.25 and 0.5%, respectively, and the $S_{z,\psi}^2$ interaction is less than 10^{-4} of the $S_{y,\psi}^2$ term. Therefore, the interaction is quite well approximated by using the propagator (18) with μt^* set to zero. Then, one obtains for arbitrary t

$$U_{\mathrm{I}}(t) = \hat{D}(\alpha(t)S_{y,\psi}) \exp\left(\mathrm{i}(\lambda t - \chi \sin(\epsilon t))S_{y,\psi}^2\right),$$

where

$$\alpha(t) = \frac{\eta\Omega}{\epsilon}(J_0 + J_2)\mathrm{e}^{-\mathrm{i}\zeta}(\mathrm{e}^{\mathrm{i}\epsilon t} - 1), \tag{24}$$

$$\lambda = \frac{\eta^2\Omega^2}{\epsilon}\left((J_0 + J_2)^2 + \frac{\epsilon}{2\delta}J_0^2\right), \tag{25}$$

$$\chi = \frac{\eta^2\Omega^2}{\epsilon^2}(J_0 + J_2)^2. \tag{26}$$

In the reference frame of the original Hamiltonian (5), the laser–ion interaction is therefore well described by the propagator

$$U(t) = \exp(-\mathrm{i}F(t)S_x)\hat{D}(\alpha(t)S_{y,\psi}) \exp\left(\mathrm{i}(\lambda t - \chi \sin(\epsilon t))S_{y,\psi}^2\right). \tag{27}$$

This propagator can be used to calculate the dynamics of expectation values of interest for the qubits. It is possible to derive simple expressions by tracing over the motional states if the vibrational mode is in a thermal state. For this, it is useful to note that $\hat{D}(\alpha(t)S_{y,\psi}) = \sum_\lambda \hat{D}(\alpha(t)\lambda)P_\lambda$ where P_λ denotes the projector on to the subspace spanned by eigenvectors of $S_{y,\psi}$ with eigenvalue λ. Moreover, the diagonal elements of the displacement operator in

the number-state representation are given by $\langle n|\hat{D}(\alpha)|n\rangle = \exp(-|\alpha|^2/2)\mathcal{L}_n(|\alpha|^2)$ where $\mathcal{L}_n$ denotes a Laguerre polynomial [20]. Since the generating function of $\mathcal{L}_n(\beta)$ is given by [21]

$$g(x,\beta) = \sum_{n=0}^{\infty} \mathcal{L}_n(\beta)x^n = \frac{1}{1-x}\exp\left(-\frac{\beta x}{1-x}\right),$$

summation over a thermal state with number state population $p_n = \frac{1}{\bar{n}+1}(\frac{\bar{n}}{\bar{n}+1})^n$ and mean phonon number $\bar{n}$ simply yields

$$\sum_n p_n\langle n|\hat{D}(\alpha)|n\rangle = \exp\left(-|\alpha|^2(\bar{n}+\tfrac{1}{2})\right).$$

In the case of two ions, $\zeta = 0$, and an initial qubit state $\rho_A = |\downarrow\downarrow\rangle\langle\downarrow\downarrow|$, the expectation value $O(t) = \text{Tr}_Q(\mathcal{O}\rho(t))$ of the observable $\mathcal{O}$ is given by

$$O(t) = \tfrac{1}{16}\text{Tr}_Q(\mathcal{O}_V\{(S_z^2 + S_x^2) - 4S_z\mathrm{e}^{-4|\alpha|^2(\bar{n}+(1/2))} + (S_z^2 - S_x^2)\mathrm{e}^{-16|\alpha|^2(\bar{n}+(1/2))}\}),$$

where Tr_Q refers to the trace of the qubit state space and $\mathcal{O}_V = V\mathcal{O}V^\dagger$ with $V(t) = \exp(-\mathrm{i}F(t)S_x)\exp(\mathrm{i}\gamma(t)S_y^2)$ and $\gamma(t) = \lambda t - \chi\sin(\epsilon t)$. As an example, the time evolution of $\langle\downarrow\downarrow|\rho(t)|\downarrow\downarrow\rangle$ is explicitly given by

$$p_{\downarrow\downarrow}(t) = \tfrac{1}{8}(2+\cos^2(2F)) + \tfrac{1}{2}\cos(2F)\cos(4\gamma)\mathrm{e}^{-4|\alpha|^2(\bar{n}+(1/2))} + \tfrac{1}{8}\cos^2(2F)\mathrm{e}^{-16|\alpha|^2(\bar{n}+(1/2))},$$

with $\alpha(t)$, $\gamma(t)$ and $F(t)$ containing the time-dependent terms. Other quantities of interest could be calculated in the same way.

A propagator similar to (27) was calculated in [11] for the case $\zeta = 0$. The authors argued that the non-resonant excitation of the carrier transition could be neglected in a first step and obtained in this way a Hamiltonian of the type described by (2) that could be integrated exactly. In a second step, they considered the influence of the previously neglected non-resonant excitations. While this treatment yields correct results for $\zeta = 0$, it fails to predict the dependence of the gate operation on ζ via the angle ψ as given by (27). Figure 4 shows the time evolution of matrix elements for the same parameters as used in [11] for the cases $\zeta = 0$ and $\zeta = \pi/2$. In the latter case, the amplitude of the non-resonant carrier oscillations is considerable and the input state $|\downarrow\downarrow\rangle$ is never perfectly mapped to a maximally entangled state. For $\zeta \neq 0$, the effect of a non-zero value of ψ is fairly small for current gate realizations using hyperfine qubits where the Lamb–Dicke parameter η is considerable. However, it becomes crucial for the realization of fast gates on optical qubits with small η since in this case the gate requires a larger value of Ω to achieve the same gate speed.

Figure 5 shows a comparison of the different propagators for the gate operation with $\eta = 0.05$ taking place in 25 trap cycles ($\delta = 0.96\nu$). For the prediction of the required coupling strength Ω for a gate operation realizing $U_{\text{id},\phi} = \exp(\mathrm{i}\frac{\pi}{8}S_{y,\psi}^2)$, equation (25) was iteratively solved to yield $\lambda t^* = \pi/8$. The propagator U_{ex} was obtained from a numerical integration of (5). Then, U_{ex} was compared to $U_{\text{id},\phi}$, to the propagator of (27), to $U_{\text{id}} = \exp(\mathrm{i}\frac{\pi}{8}S_y^2)$ and to the prediction $U_{\text{pert}} = \exp(\mathrm{i}2\pi\eta^2\Omega^2/\epsilon^2 S_y^2)$ of second-order perturbation theory. Since the exact propagator does not perfectly return the motional state to the initial state at the end of the gate, the following procedure was applied for the calculation of the distance d between the propagators: we assume that the ions are initially in the motional ground state and that a cooling mechanisms returns the motional state to the ground state at the end of the gate operation without
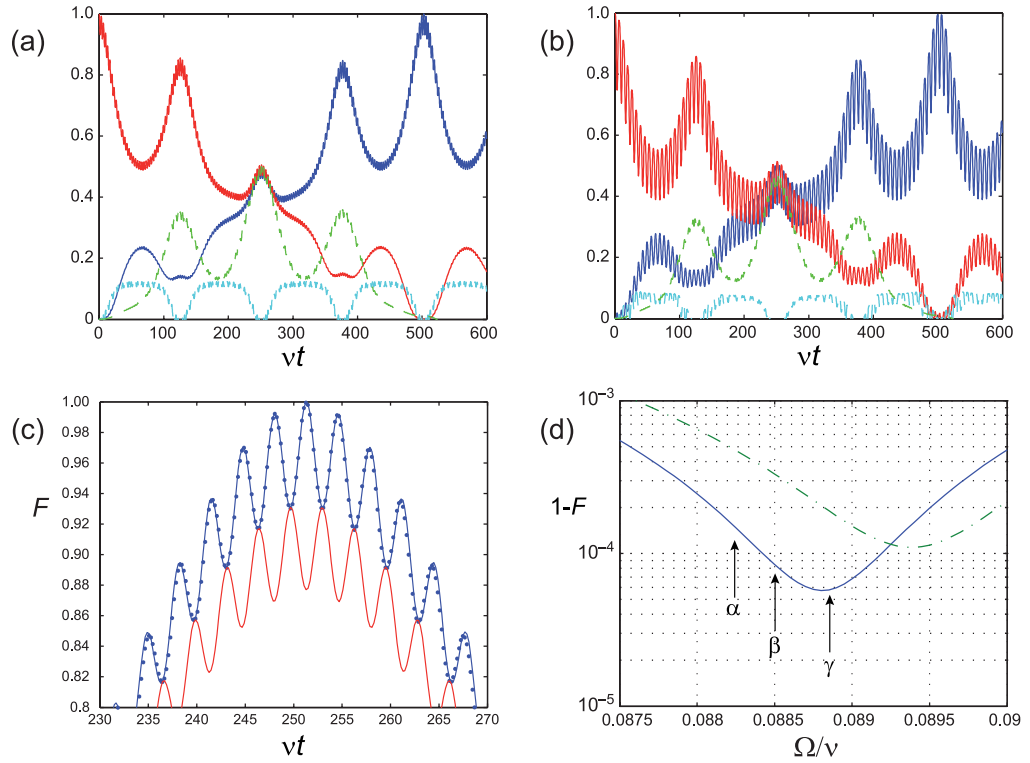
Figure 4. (a) Time evolution of the density matrix elements of two ions in a thermal state with $\bar{n} = 2$ undergoing a Mølmer–Sørensen interaction with $\Omega = 0.0885\,\nu$, $\eta = 0.1$, $\epsilon = 0.05\,\nu$ and $\zeta = 0$. The calculations are based on (27). The values chosen reproduce the curves shown in figure 3(b) of [11]. Counting from above at $\nu t = 60$, the curves represent the populations $\rho_{\downarrow\downarrow,\downarrow\downarrow}$, $\rho_{\uparrow\uparrow,\uparrow\uparrow}$ and the coherences $\mathrm{Im}(\rho_{\downarrow\downarrow,\uparrow\uparrow})$ and $\mathrm{Re}(\rho_{\downarrow\downarrow,\uparrow\uparrow})$. At $\nu t \approx 250$ ($t = 4\pi/\epsilon$), the ions are in a maximally entangled state. (b) Same as (a) but with $\zeta = \pi/2$. If the gate operation starts in an intensity minimum of the amplitude-modulated laser beam, the non-resonant carrier oscillations are much stronger. At $\nu t = 250$, the quantum state is no longer maximally entangled. (c) Fidelity $F = \langle \psi_{\max} | \rho(t) | \psi_{\max} \rangle$ of creating the maximally entangled state $|\psi_{\max}\rangle = (|\downarrow\downarrow\rangle - \mathrm{i}|\uparrow\uparrow\rangle)/\sqrt{2}$ near the optimum calculated from (27). The upper curve corresponds to $\zeta = 0$, the lower one to $\zeta = \pi/2$. The points on top of the upper curve represent the fidelity for $\zeta = 0$ and were obtained by a numerical integration of the Hamiltonian (5) after applying the Lamb–Dicke approximation. (d) Infidelity $1 - F$ of the gate at $\nu t = 250$ for $\zeta = 0$ and a state with $\bar{n} = 0$. The solid line is a numerical integration of (5) in the Lamb–Dicke approximation, the dash-dotted line is based on the full Hamiltonian. The arrow labelled 'α' denotes the optimum Rabi frequency predicted by (21), 'β' the value of Ω chosen in [11], 'γ' the Rabi frequency predicted by (25).

affecting the qubit states. This turns the unitary evolution into a quantum process acting only on the internal states of the ions. For the comparison of two quantum processes $\mathcal{E}_1 \mathcal{E}_2$, the processes are mapped using the Jamiolkowski isomorphism on to density matrices ρ_1 and ρ_2 for which the distance $d(\rho_1, \rho_2) = 1 - \mathrm{Tr}(\sqrt{\sqrt{\rho_1}\rho_2\sqrt{\rho_1}})$ is calculated [22, 23]. The results show that the
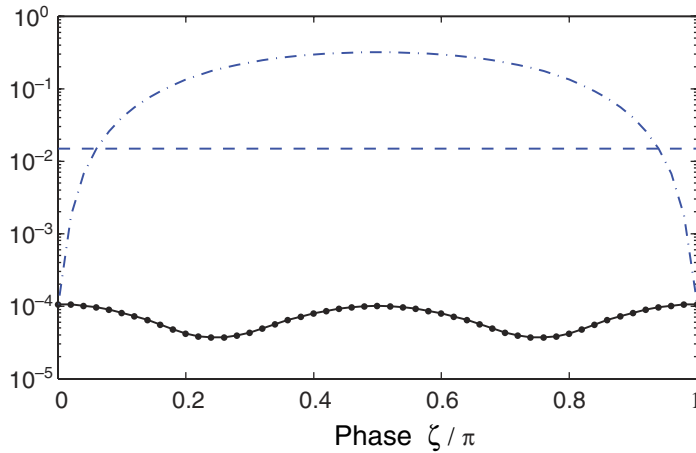
Figure 5. Performance of the $\sigma_\phi \otimes \sigma_\phi$ gate as a function of the phase ζ for a gate operation taking place in 25 trap cycles with $\eta = 0.05$, $\delta = 0.96\nu$ and $\Omega = 0.221\nu$. The figure shows the distance $d(U_{\text{ex}}, U_{\text{id},\phi})$ between the exact propagator U_{ex} obtained by numerical integration of (5) and the gate operation $U_{\text{id},\phi} = \exp(\text{i}\frac{\pi}{8} S_y^2)$ (solid line). The points on top of the line denote $d(U_{\text{ex}}, U_{(27)})$ where $U_{(27)}$ is the propagator given by (27), thus demonstrating that this equation is a very good approximation to the exact solution. The dashed-dotted line shows $d(U_{\text{ex}}, U_{\text{id},\phi})$ with $U_{\text{id},\phi} = \exp(\text{i}\frac{\pi}{8} S_y^2)$ and the dotted line $d(U_{\text{ex}}, U_{\text{pert}})$ with $U_{\text{pert}} = \exp(\text{i}2\pi\eta^2\Omega^2/\epsilon^2 S_y^2)$ as predicted by simple second-order perturbation theory. More details regarding the distance measure d are given in the text.

propagator given by (27) correctly predicts the coupling strength as well as the operator realized by the gate operation. It also becomes obvious that U_{id} considerably deviates from the operation generated by the Hamiltonian (5) unless $\zeta = 0$.

3.3. Comparison of $\sigma_z \otimes \sigma_z$ and $\sigma_\phi \otimes \sigma_\phi$ gates

The main advantage of the $\sigma_z \otimes \sigma_z$ interaction on optical qubits appears to be its insensitivity to changes in the optical path length. In the limit of weak excitation, the gate operation tolerates changes that occur within the gate operation as in each elementary process a photon is absorbed and another one emitted into the same laser beam (this property does not hold for hyperfine qubits since here Raman beams in a counter-propagating configuration are used). If higher Rabi frequencies are used, the interaction rather becomes $\sigma_{z,\psi} \otimes \sigma_{z,\psi}$ which make it susceptible to path-length fluctuations within the gate time. Still, if amplitude-shaped pulses are applied (see section 4), the gate operation tolerates changes of the path length that occur between consecutive applications of the gate. This is not the case for the Mølmer–Sørensen gate which becomes robust against changes between gate operations but remains susceptible to changes occurring within the gate when the gate is sandwiched between $\pi/2$ pulses applied to both qubits.

The $\sigma_z \otimes \sigma_z$ gate, however, seems to be much less favourable with respect to the following criteria: (i) the Rabi frequency that is required for performing the gate operation in a given time, (ii) the strength of saturation effects reducing the coupling for the Rabi frequency needed for

Table 1. Comparison of $\sigma_z \otimes \sigma_z$ and $\sigma_\phi \otimes \sigma_\phi$ gates. The first row gives the Rabi frequency Ω required to perform an entangling gate operation as a function of η and the gate duration. The latter is expressed as the number of trap oscillation periods N_t. The second row lists the reduction in coupling strength for this kind of gate due to saturation effects. The third row compares the unwanted to the desired coupling strength.

Gate type	$\sigma_z \otimes \sigma_z$	$\sigma_\phi \otimes \sigma_\phi$
Rabi frequency	$\Omega/\nu = 1/(4\sqrt{\eta N_t})$	$\Omega/\nu = 1/(4\eta N_t)$
Saturation strength	$\gamma = 2/(3\eta N_t)$	$\gamma = 1/(4\eta^2 N_t^2)$
Coupling ratio	$\kappa/\theta = 8/(3\eta)$	$\mu/\lambda = 1/(6\eta^2 N_t^3)$

the gate operation, and (iii) the ratio between the desired and the unwanted spin–spin couplings. Table 1 shows a comparison of the gates with respect to these criteria, thus summarizing the results (11), (12) and (15) for the $\sigma_z \otimes \sigma_z$ gate and (21), (22) and (23) for the $\sigma_\phi \otimes \sigma_\phi$ gate. For all three criteria, the Mølmer–Sørensen performs better. Having a low Rabi frequency is also of interest when it comes to non-resonant excitation of other vibrational modes or light shifts induced by excitation of far-detuned dipole transitions.

4. Amplitude-shaped pulses and spin echos

4.1. Amplitude-shaped laser pulses

In the limit of fast gate operations, the Hamiltonians (10) and (17) become sensitive to the phase ζ which is related to the intensity of the bichromatic laser field at the start of the gate operation. It is therefore interesting to shape the intensity of the bichromatic laser field during the gate operation so that the atomic operator $\mathcal{O}(t) = S_{j,\psi(t)}$, with $\psi(t) = \frac{4\Omega(t)}{\delta}\sin\zeta$, appearing in the Hamiltonians becomes time-dependent but independent of ζ at the beginning and at the end of the gate when the intensity is low. In this way, the gate could be made insensitive to ζ by an adiabatic process where $\mathcal{O}(t)$ evolves from S_j at the start of the gate operations to a ζ-dependent operator $S_{j,\psi(t)}$ and back to S_j. However, the state $\alpha(t)$ of the vibrational mode generally does not return to its original state at the end of the gate under the action of the propagator (3) when the coupling $\gamma(t)$ is made time-dependent. There is, however, a class of shaped pulses with the property $\alpha(\tau) = 0$ that can be constructed in the following way: by applying an amplitude-shaped pulse twice with a sign change in the coupling between the two pulses, i.e. $\gamma_2(t) = -\gamma_1(t)$, one obtains the propagator

$$U = U_{-\gamma}(2\tau, \tau)U_\gamma(\tau, 0) = \exp(\mathrm{i}2\Phi(\tau)\mathcal{O}^2),$$

because the first and the second pulse displace the motional state into opposite directions but by an equal amount (see (3)). A quantum state that is displaced along a circle in phase space by an off-resonant force of constant magnitude, $\gamma(t) = \Omega e^{\mathrm{i}\epsilon t}$, $t \in [0, 2\pi/\epsilon]$, can be viewed as a special case of this pulse form with $\tau = \pi/\epsilon$. For the bichromatic gates based on the interactions (10) and (17), the sign change can be accomplished by either shifting the phase ζ during the action of the second pulse by an amount $\pi/2$ (π), respectively, or by changing the overall phase of the laser by π during the second pulse (i.e. $\Omega \to -\Omega$).

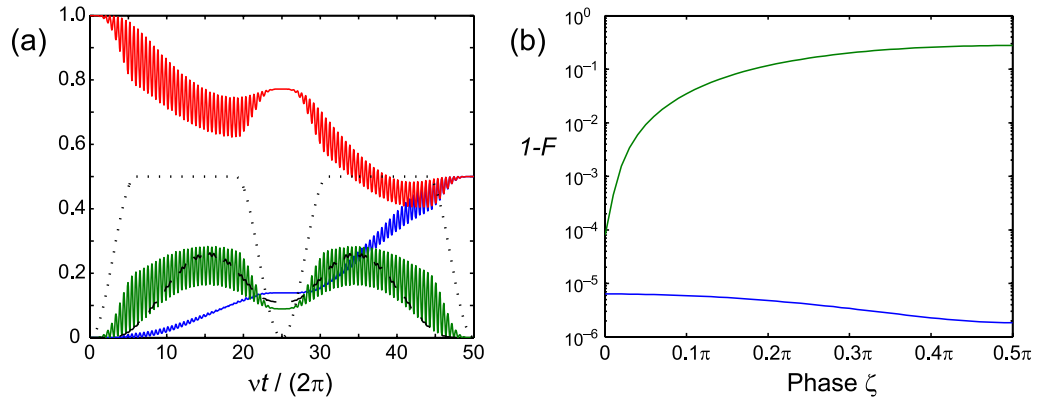**IOP** Institute of Physics Φ DEUTSCHE PHYSIKALISCHE GESELLSCHAFT

Figure 6. Mølmer–Sørensen gate operation with two amplitude-shaped laser pulses based on the full Hamiltonian (5) without Lamb–Dicke approximation. For parameters $\Omega_{\mathrm{max}} = \max(|\Omega|) = 0.167\,\nu$, $\eta = 0.05$, the gate takes place during 50 trap oscillation periods. The pulses are switched on and off during eight trap cycles using a $\cos^2$-profile. During the second pulse, the phase of the blue- and the red-detuned beam is shifted by π with respect to the first pulse. (a) Time evolution of the populations $p_{\uparrow\uparrow}$, $p_{\downarrow\downarrow}$, $p_{\downarrow\uparrow} + p_{\uparrow\downarrow}$, when starting from state $|\uparrow\uparrow, n = 0\rangle$ at time $t = 0$. The dotted line shows the coupling strength $|\Omega(t)|/(2\Omega_{\mathrm{max}})$, the dashed line is the average number of vibrational quanta. (b) Infidelity of the final state as a function of the phase ζ. The upper curve shows the strong influence of the phase for a gate operation with constant coupling strength $\Omega = 0.147\,\nu$ where a high-fidelity operation is achieved only for $\zeta = 0$. For the amplitude-shaped gate, the fidelity is practically independent of ζ. Similar results are also obtained for other input states. For a realistic calculation of F, decoherence caused by spontaneous decay of the metastable state would have to be taken into account.

Figure 6 illustrates the use of amplitude-shaping in order to make the Mølmer–Sørensen gate operation robust against fluctuations in the phase ζ between the blue- and the red-detuned laser beam. In this example, an entangling gate is accomplished within $N = 50$ trap oscillation periods by a pair of laser pulses with $\Omega(t + \tau) = -\Omega(t)$, for $t \leqslant \tau$ with $\tau = \pi N/\nu$. As shown in figure 6(a), the pulses are switched on and off within eight trap cycles. After the first pulse, the vibrational state has not returned to its initial state. It is only after the second pulse that the correlations between the vibrational state and the qubit states vanish again. Using this technique, the initial state $|\uparrow\uparrow, n = 0\rangle$ is mapped to the target state $\frac{1}{\sqrt{2}}(|\uparrow\uparrow\rangle + \mathrm{i}|\downarrow\downarrow\rangle)|n = 0\rangle$ with an infidelity of below 10^{-5} (see figure 6(b)). This is in sharp contrast to the case of an excitation of the same duration with constant amplitude where the infidelity depends on the phase ζ and varies between 10^{-4} and 0.2. Similar results are also obtained for other input states.

4.2. Spin echos

Spin echo pulses can be combined with amplitude-shaped laser pulses to make the $\sigma_z \otimes \sigma_z$ gate more robust against imperfections. It is possible to implement the conditional phase gate operation by having the motional state perform two circles in phase space so that the gate pulse can be split up into two separate pulses. Since the quantum states $|\uparrow\uparrow\rangle$, $|\downarrow\downarrow\rangle$ as well as the

states $|{\uparrow}{\downarrow}\rangle$, $|{\downarrow}{\uparrow}\rangle$ pick up the same phases $\Phi_{\uparrow\uparrow} = \Phi_{\downarrow\downarrow}$, $\Phi_{\uparrow\downarrow} = \Phi_{\downarrow\uparrow}$, it is possible to exchange the states $|{\uparrow}{\uparrow}\rangle \leftrightarrow |{\downarrow}{\downarrow}\rangle$, $|{\downarrow}{\uparrow}\rangle \leftrightarrow |{\uparrow}{\downarrow}\rangle$ by a collective π-pulse sandwiched between the two gate pulses and to exchange the populations at the end of the gate sequence again. The first spin-echo π-pulse inverts the direction of the force on the motional state so that the motional state returns to the initial state after the second spin-dependent pulse. In contrast to the case of shaped pulses without spin-echo, there is no need to change the phase ζ of the second pulse or the sign of the coupling strength Ω. The spin echo procedure is advantageous for the following reasons:

1. The gate becomes more robust against unequal light intensities on the ions.

2. Single qubit phases arising from light shifts are transformed into an unimportant global phase. In the context of this gate, light shifts will mainly be due to an imbalance in the power of the blue- and the red-detuned laser beams and also due to very off-resonant excitation of dipole transitions. In addition, a light shift δ_{ls} occurs if the average frequency ω_L of the bichromatic light field does not exactly coincide with the atomic transition frequency ω_0. However, this light shift will be fairly small as $\delta_{ls} \propto (\Omega/\delta)^2(\omega_L - \omega_0)$.

3. Collective spin flips arising from the term S_y^2 in (10) can be cancelled to first order by choosing rotation axes for the π-pulses on ion 1 and ion 2 that differ by $90°$ (x-rotation on ion 1 and y-rotation on ion 2). This effectively changes the sign of the rotation angle κ occurring in (13) for the second pulse and eliminates the spin flip contribution of the interaction. To perform different π-pulses on both ions requires, however, either a different trap frequency that changes the distance between the ions by $\lambda/4$ or an additional laser beam.

In the limit of short gate operations, spin echos become somewhat less efficient in cancelling perturbations described by S_z interactions as the gate interaction $\propto S_{z,\psi}^2$ no longer commutes with S_z for $\psi \neq 0$.

For the Mølmer–Sørensen gate operation, where $[S_{y,\psi}^2, S_z]$ is not a small quantity, spin echos seem to be of limited use. If, however, the gate interaction is sandwiched between a pair of collective $\pi/2$ pulses to turn it into a $\sigma_z \otimes \sigma_z$ interaction, spin echos are helpful for cancelling perturbations occurring between consecutive gates. Also, it should be noted that a spin-echo like technique was already proposed in [10] in order to cope with number-state dependent ac-Stark shifts that arise if the gate is implemented by illuminating ion 1 with a red-detuned laser beam and ion 2 with a blue-detuned laser beam instead of using a bichromatic light field for both ions.

5. Conclusions

Collective laser–ion interactions with bichromatic laser beams are capable of performing both $\sigma_z \otimes \sigma_z$ gates as well as Mølmer–Sørensen gate operations. The analysis shows that it is important to include non-resonant excitation of the carrier transition for the precise calculation of the gate operation. While the paper was focused on the case of qubit states linked by a weak optical transition, the discussion of the Mølmer–Sørensen gate interaction applies also to hyperfine qubits where non-resonant carrier excitation also occurs in the limit of fast gate operations. For optical qubits, the required laser beams are chosen to be co-propagating which allows for a robust and experimentally easily realizable set-up where an acousto–optical modulator is used in single-pass configuration to create the bichromatic light field. In a direct comparison of the gates, the Mølmer–Sørensen interaction seems to be advantageous in terms

of required laser power and gate accuracy while the $\sigma_z \otimes \sigma_z$ interaction has the advantage of being robust even against certain path length fluctuations occurring during the gate operation in the limit of weak driving where $S_{z,\psi} \approx S_z$. For gate durations coming close to $T = 2\pi/(\eta\nu)$, control of the phase ζ between the red- and the blue-detuned laser beams is of vital importance unless the gate is performed using amplitude-shaped laser pulses. In this case, the requirements are strongly relaxed and the gates appear to be very promising for experimental realization. The possibility of using a single laser beam for global single qubit and entangling operations also opens interesting perspectives for creating multi-particle entangled states with more than two ions. The operations using this beam could be combined with an off-resonant strongly focused beam capable of inducing σ_z operations on individual qubits in order to create a larger variety of complex entangled states.

Acknowledgments

References

[1] Nielsen M A and Chuang I L 2000 *Quantum Computation and Quantum Information* (Cambridge: Cambridge University Press)
[2] Schmidt-Kaler F *et al* 2003 *Nature* **422** 408
[3] Leibfried D *et al* 2003 *Nature* **422** 412
[4] Haljan P C *et al* 2005 *Phys. Rev.* A **72** 062316
[5] Home J P *et al* 2006 *New J. Phys.* **8** 188
[6] Cirac J I and Zoller P 1995 *Phys. Rev. Lett.* **74** 4091
[7] Monroe C, Meekhoff D M, King B E, Itano W M and Wineland D J 1995 *Phys. Rev. Lett.* **75** 4714
[8] Milburn G J 1999 *Preprint* quant-ph/9908037
[9] Milburn G J, Schneider S and James D F V 2000 *Fortschr. Phys.* **48** 801
[10] Sørensen A and Mølmer K 1999 *Phys. Rev. Lett.* **82** 1971
[11] Sørensen A and Mølmer K 2000 *Phys. Rev.* A **62** 022311
[12] Solano E, de Matos Filho R L and Zagury N 1999 *Phys. Rev.* A **59** R2539
[13] Leibfried D, Blatt R, Monroe C and Wineland D J 2003 *Rev. Mod. Phys.* **75** 281
[14] Monroe C M, Meekhof D M, King B E and Wineland D J 1996 *Science* **272** 1131
[15] Wallentowitz S and Vogel W 1995 *Phys. Rev. Lett.* **75** 2932
[16] Solano E, de Matos Filho R L and Zagury N 2001 *Phys. Rev. Lett.* **87** 060402
[17] Kim K *et al* 2007 *Preprint* 0710.3950
[18] Lee P J, Brickman K-A, Deslauriers L, Haljan P C, Duan L-M and Monroe C 2005 *J. Opt. B: Quantum Semiclass. Opt.* **7** S371
[19] Magnus W 1954 *Commun. Pure Appl. Math.* **7** 649
[20] Cahill K E and Glauber R J 1969 *Phys. Rev.* **177** 1857
[21] Abramowitz M and Stegun I A 1972 *Handbook of Mathematical Functions* (New York: Dover) p 784
[22] Gilchrist A, Langford N K and Nielsen M A 2005 *Phys. Rev.* A **71** 062310
[23] Dür W, Hein M, Cirac J I and Briegel H-J 2005 *Phys. Rev.* A **72** 052326